SIMULATION OF CONTINUOUS CASTING OF STEEL UNDER THE INFLUENCE OF MAGNETIC FIELD USING THE LOCAL-RADIAL BASIS-FUNCTION COLLOCATION METHOD

SIMULACIJA KONTINUIRNEGA ULIVANJA JEKLA POD VPLIVOM MAGNETNEGA POLJA NA PODLAGI METODE KOLOKACIJE Z RADIALNIMI BAZNIMI FUNKCIJAMI

Katarina Mramor[1], Robert Vertnik[2,3], Božidar Šarler[1,3,4]

[1]CO BIK, Tovarniška c. 26, 5270 Ajdovščina, Slovenia
[2]Štore Steel, Železarska c. 3, 3220 Štore, Slovenia
[3]University of Nova Gorica, Vipavska 13, 5000 Nova Gorica, Slovenia
[4]Institute of Metals and Technology, Lepi pot 11, 1000 Ljubljana, Slovenia
katarina.mramor@cobik.si

The initial results obtained with the local-radial basis-function collocation method (LRBFCM) for a two-dimensional (2D), simplified model of continuous casting of steel with an externally applied magnetic field are presented. The multiphysics model is composed of turbulent-solidification equations (mass, momentum, energy, turbulent kinetic energy, turbulent dissipation rate) and Maxwell's equations that are numerically solved for the non-uniform node arrangement. The numerical procedure is structured using the explicit time stepping and local collocation with multiquadric radial basis functions (MQ RBF) on the overlapping five-node subdomains. The pressure-velocity coupling follows the fractional-step method (FSM) and the convection is treated with adaptive upwinding.
The novel LRBFCM has been already verified in several benchmark test cases, such as the natural convection in a cavity with a magnetic field, the lid-driven cavity, and the flow over the backward-facing step with a transverse magnetic field.

Keywords: continuous casting of steel, turbulent flow, solidification, magnetohydrodynamics

Namen članka je predstavitev prvih rezultatov s poenostavljenim 2D-modelom za kontinuirano ulivanje jekel pri zunanjem magnetnem polju, izračunanih z metodo kolokacije z radialnimi baznimi funkcijami. Numerični model združuje Navier-Stokesove in Maxwellove enačbe, ki jih rešujemo na neenakomerni porazdelitvi točk. V numeričnem postopku je uporabljena eksplicitna časovna shema na pettočkovnih poddomenah, na katerih so uporabljene multikvadrične radialne bazne funkcije. Sklopitev tlaka in hitrosti se rešuje z metodo delnih korakov.
Omenjeno metodo smo poprej verificirali za izračun različnih preizkusov, kot so naravna konvekcija v kotanji z magnetnim poljem, kotanja z vsiljenim tokom ter tok preko stopnice v kanalu z magnetnim poljem. Dobljeni rezultati kažejo dobro ujemanje z drugimi numeričnimi postopki, kot je npr. metoda končnih volumnov.

Ključne besede: kontinuirano ulivanje jekla, turbulenten tok, strjevanje, magnetohidrodinamika

1 INTRODUCTION

The production of continuously cast steel[1] has greatly expanded in recent years. Continuous casting of billets, blooms and slabs is the most common process of steel production.[2] The continuously growing demand for cast steel has fueled the need to produce the steel of even better quality. Although the process of continuous casting of steel is cost efficient, exhibiting a high yield and good quality of the products, it can be further improved by introducing the electromagnetic (EM) field into it. The EM force, which is a result of an applied magnetic field, affects the velocity and temperature fields. By adjusting the magnetic field, the amount of defects in the material can be significantly reduced.

The magnitudes of the velocity, the temperature and magnetic fields are all crucial to the final quality of a product. As all these quantities are difficult or impossible to measure, numerical models help us to better understand and further improve the process. A number of different numerical models[3] have so far been used in the simulations of the problem. They include the finite-volume method (FVM),[4–8] the finite-element method (FEM)[9] and some more advanced meshless methods like the local-radial basis-function collocation method (LRBFCM).[10]

2 GOVERNING EQUATIONS

The system of governing equations that describes the turbulent heat transfer and the fluid flow as well as the magnetic field in the continuous casting of steel, is based on the Reynolds time-averaging approach to modeling a turbulent flow[11] and a mixture-continuum model, first introduced by Bennon and Incropera.[12] The system consists of five time-averaged mixture equations:

$$\nabla \cdot \mathbf{v} = 0 \tag{1}$$

$$\rho \frac{\partial \mathbf{v}}{\partial t} + \rho \nabla(\mathbf{v}\mathbf{v}) = -\nabla p + \nabla[(\mu_L + \mu_t)[\nabla \mathbf{v} + (\nabla \mathbf{v})^T]] -$$
$$-\frac{2}{3}\rho \nabla k - \frac{\mu_L(1-f_L)^2}{Cf_L^3}(\mathbf{v}-\mathbf{v}_s) + \rho \beta_T g(T-T_{ref}) + \mathbf{F}_m \qquad (2)$$

$$\rho \frac{\partial h}{\partial t} + \rho \nabla(\mathbf{v}h) = \nabla(\lambda \nabla T) + \nabla(\mathbf{v}h - f_S\mathbf{v}_S h_S -$$
$$-f_L\mathbf{v}_L h_L) + \nabla\left(f_L \frac{\rho_L \nu_t}{\sigma_t}\nabla h_L\right) \qquad (3)$$

$$\rho \frac{\partial k}{\partial t} + \rho \nabla(\mathbf{v}k) = \nabla\left[\left(\mu_L + \frac{\mu_t}{\sigma_k}\right)\nabla k\right] + P_k + G_k -$$
$$-\rho\varepsilon + \rho D - \mu_L \frac{(1-f_L)^2}{Cf_L^3}k \qquad (4)$$

$$\rho \frac{\partial \varepsilon}{\partial t} + \rho \nabla(\mathbf{v}\varepsilon) = \nabla\left[\left(\mu_L + \frac{\mu_t}{\sigma_\varepsilon}\right)\nabla\varepsilon\right] + \rho E -$$
$$-\mu_L \frac{(1-f_L)^2}{Cf_L^3}\varepsilon + \left[c_{1\varepsilon}f_1(P_k + c_{3\varepsilon}G_k) - c_{2\varepsilon}f_2\rho\varepsilon\right]\frac{\varepsilon}{k} \qquad (5)$$

where $\mathbf{v}$ is the velocity of the mixture, $\rho = \rho_S = \rho_L$ is the density of the mixture, assumed to be constant; t stands for the time and p for the pressure; μ_t is the turbulent viscosity and μ_L is the dynamic viscosity; k represents the turbulent kinetic energy and K is the permeability of the porous matrix. β_T, g, T, and T_{ref} represent the thermal-expansion coefficient, the gravitational acceleration, the temperature and the reference temperature, respectively. $\mathbf{F}_m$ stands for the Lorentz force, h for the enthalpy and λ for the thermal conductivity. f_S, f_L, $\mathbf{v}_S$, $\mathbf{v}_L$, h_S, and h_L represent the solid-volume fraction, the liquid-volume fraction, the velocity of the solid phase, the velocity of the liquid phase, the enthalpy of the solid phase and the enthalpy of the liquid phase, while ν_t is the turbulent kinematic viscosity. Symbols ε and C stand for the dissipation rate and the morphology constant of the porous media. Symbols σ_t, σ_k, σ_ε, $c_{1\varepsilon}$, f_1, $c_{2\varepsilon}$ and f_2 are the closure coefficients of the turbulence model. P_k, G_k, D and E are the shear production of the turbulent kinetic energy, the generation of turbulence due to the buoyancy force, the source term in the k equation and the source term in the ε equation, respectively. The closure relations defined by Abe, Kondoh and Nagano[13] are used in the present work. A detailed description of the closure coefficients, source terms and damping functions are given in the paper by Šarler et al[14]. The Lorentz force is defined as:

$$\mathbf{F}_m = \mathbf{j} \times \mathbf{B} \qquad (6)$$

where $\mathbf{j}$ and $\mathbf{B}$ are the current density and the magnetic-flux density. Maxwell's equations are used to calculate the current density:

$$\mathbf{j} = \sigma(-\nabla\phi + \mathbf{v} \times \mathbf{B}) \qquad (7)$$

where σ is the fluid electric conductivity, ϕ is the fluid electric potential and B is the externally applied magnetic field. The induced magnetic field is assumed negligible in comparison with the applied magnetic field.

2.1 Initial and boundary conditions

The governing equations are strongly coupled. For the steady solution of a problem it is, therefore, very important how the initial conditions are chosen in order to minimize the required iterations to reach the steady state. Five different boundaries are chosen: the inlet, free surface, wall, outlet and symmetry of the present model. A detailed description of the initial and boundary conditions are given in the article by Šarler at al[14]. The model of the domain is presented in **Figure 1** and the computational domain is depicted in **Figure 2**.

3 SOLUTION PROCEDURE

The solution of the governing equations is obtained with the LRBFCM employing the explicit time stepping. The fractional-step method (FSM)[15] is used to solve the pressure-velocity coupling and an upwinding scheme is used to stabilize the highly convective situation.[16]

The solution procedure begins by calculating the initial Lorentz force (equation (6)). Afterwards, the intermediate velocity is calculated, without a pressure gradient. The pressure is then calculated from the Poisson equation[14] by assembling and solving a sparse matrix.[17] The calculated pressure gradient is afterwards used to correct the intermediate velocities. After the solution of the velocity field, the equations for the turbulent kinetic energy and dissipation rate are solved. This is followed
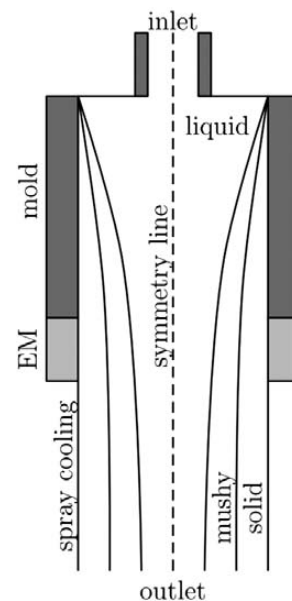
Figure 1: Simplified 2D model of continuous casting of steel
Slika 1: Poenostavljeni 2D-model kontinuirnega ulivanja jekla
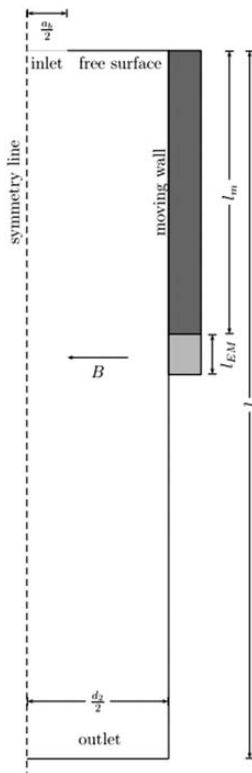
Figure 2: Scheme of the computational domain
Slika 2: Shema računske domene

by the solution of the enthalpy equation. The temperature is calculated from the enthalpy, using the temperature-enthalpy constitutive relation.[17,18] Finally, the turbulent viscosity, velocity, temperature, turbulent kinetic energy and dissipation rate are updated and the solution is ready for the next time step.

The LRBFCM is structured in the following way: Approximation function θ is represented on each of the subdomains as a linear combination of the radial basis functions (RBFs) as:

$$q(_l\mathbf{p}_n) = \sum_{i=1}^{M} {}_l\psi_i(_l\mathbf{p}_n) {}_l\gamma_i \tag{8}$$

where $_l\psi_i$, $_l\gamma_i$, and M represent the RBF shape functions, centred in points $_l\mathbf{p}_n$, the expansion coefficients, and the number of shape functions, respectively. The most commonly used RBF is the multiquadric RBF:[19,20]

$$_l\psi_i(\mathbf{p}) = \sqrt{_l r_i^2(\mathbf{p}) + c^2} \tag{9}$$

where c stands for the dimensionless shape parameter, set to 32 in all the calculations, and the distance between the nodes:

$$_l r_i^2(\mathbf{p}) = \sqrt{\left(\frac{x - x_i}{_l x_{i\max}}\right)^2 + \left(\frac{y - y_i}{_l y_{i\max}}\right)^2} \tag{10}$$

is scaled with $_l x_{i\max}$ and $_l y_{i\max}$, the scaling parameters of subdomain l in the x and y directions, respectively (**Figure 3**).

A subdomain is formed around each of the calculation points consisting of the $_l M - 1$ nodes nearest to node $_l\mathbf{p}_n$. For the purpose of this work, five-node overlapping subdomains are used. By considering the collocation condition of:

$$_l\theta(_l\mathbf{p}_n) = \theta_{i(l,n)} \tag{11}$$

a linear system of equations is obtained. To solve the partial differential equations (PDEs), the first and second derivatives of function $_l\theta(\mathbf{p})$ have to be calculated:

$$\frac{\partial^j}{\partial \chi^j} {}_l\theta(\mathbf{p}) = \sum_{i=1}^{M} \frac{\partial^j}{\partial \chi^j} {}_l\psi_i(\mathbf{p}) {}_l\gamma_i \tag{12}$$

where index $j = 1,2$ is used to denote the order of the derivative and $\chi = x,y$. A detailed explanation of the solution procedure is given in the paper by Vertnik et al.[17,18] The schematics of the discretization scheme is shown in **Figure 3**.

4 NUMERICAL IMPLEMENTATION

The sparse-pressure matrices, used for the solution of the pressure and the flux-density Poisson equations, are solved by applying the Pardiso routine and Intel Math Kernel Library 11. The OpenMP Library is used for the parallelization. The post processing is performed in PGPlot, Gnuplot 4.4 and Octave 3.6.1. The results were calculated on an HP Proliant DL380 G/7 server running on 64 bit MS Windows.

5 NUMERICAL EXAMPLES

The numerical procedure has so far been verified on the following benchmark test cases: the lid-driven cavity,[21] the natural convection in a cavity,[22] and the backward-facing step.[23] The lid-driven test case was used
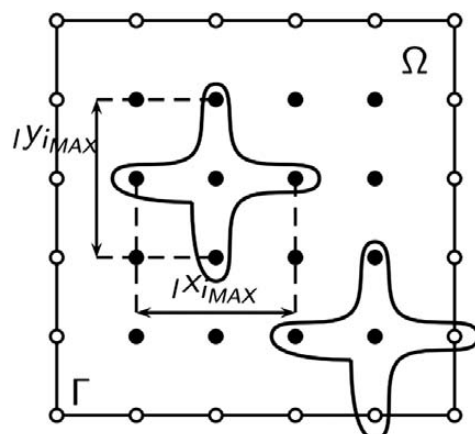
Figure 3: Discretization scheme. Γ, Ω, $_l x_{i\mathrm{MAX}}$ and $_l y_{i\mathrm{MAX}}$ represent the boundary, domain and scaling parameters in the x and y directions, respectively. The circles represent the boundary nodes, whereas the black dots represent the domain nodes.
Slika 3: Diskretizacijska shema. Γ, Ω, $_l x_{i\mathrm{MAX}}$ in $_l y_{i\mathrm{MAX}}$ označujejo rob, območje ter skalirna parametra v smeri x in y. Robne točke so označene s krogci, območne točke pa s pikami.

to verify the coupling between the mass and momentum equations.[21] In the natural-convection case, the energy-conservation equation was added.[22] For the backward-facing step problem, the boundary conditions for the inflow and outflow problems were tested. The natural-convection and backward-facing-step problems were first tested without a magnetic field and then with an external magnetic field. The results of all of the test cases are in good agreement with the reference results, calculated with a commercial code or obtained from several published sources. Since the results of our calculations, mentioned in the above history of test cases, are in good agreement with the reference results, the method is subsequently applied to the simplified problem of continuous casting of steel with a magnetic field, as defined in the paper by Šarler et al.[14]

5.1 Continuous-casting geometry and material properties

The simplified 2D continuous-casting model geometry is shown in **Figure 1** and the elements of the discretization are presented in **Figure 2**. The computational domain coincides with a half of the longitudinal section of the billet, taken to be 1.8 m long and 14 cm wide. The SEN diameter is 3.5 cm, the mold height is 0.8 m and the EM-coil height is 10 cm. The material properties of steel are temperature and steel grade dependent. However, for the purpose of the present simplified model, constant values are used. The values are given in **Table 1**.

Table 1: Simplified material properties of steel
Tabela 1: Poenostavljene snovne lastnosti jekla

| Property	Value
ρ	7200 kg/m^3
λ	30 W/(m K)
c_p	700 J/(kg K)
T_S	1680 K
T_L	1760 K
h_m	250000 J/kg
μ	0.006 Pa s
β_T	$1 \cdot 10^{-4}$ K^{-1}
C	$1.6 \cdot 10^8$ m^{-2}

The results of the numerical simulation are represented in the following sections of the paper.

5.2 Convergence of the method and a comparison with the reference results for the continuous-casting process

First the convergence of the method was tested for the node arrangements with 20 220, 50 951, 73 940, 100 089, 131 452, 165 426 non-uniformly arranged nodes. The convergence was tested for the velocity and the temperature fields. The vertical and horizontal components of the velocity were compared for three different vertical cross-sections: just before the application of the mag-

netic field, just after the application of the magnetic field and at the end of the computational domain, as can be seen in **Figure 4** (left). The temperature was verified at two different vertical directions, the one at the center of the domain and the one at the outside wall, as shown in **Figure 4** (right).

As can be seen in **Figures 5** to **12**, the smallest appropriate node arrangement is 100 089. The results were also compared with the results obtained with the commercial code based on the FVM (Fluent[23]). The smallest appropriate amount of the finite volumes in the commercial code for reaching a reasonable convergence was 169 169. The agreement of the velocity profiles with the commercial code (the solid line denoted with F) is similarly good for the horizontal as well as vertical velocities. The largest differences occur at the positions closer to the inlet. At the positions closer to the end of the computational domain, where a fully developed flow and a partial solidification take place, the agreement between the results obtained with the LRBFCM and FVM is excellent. In the early stages of the flow, slightly larger differences can be observed. The differences between the commercial-code results and the results obtained with the in-house built LRBFCM are reasonably small. The exact cause for the differences is
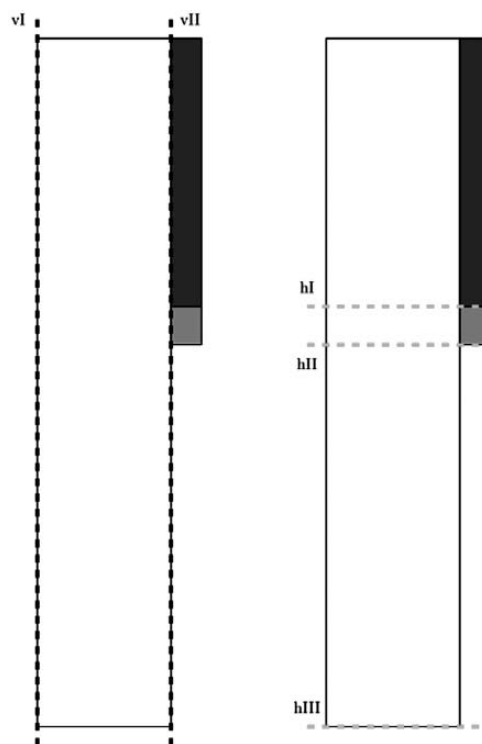
Figure 4: Left: the positions of the velocity-field comparison lines; hI = –0.8 m, hII = –0.9 m, hIII = –1.8 m. Right: the positions of the temperature-field comparison lines; vI = 0.0 m (centreline), vII = 0.07 m (surface).
Slika 4: Levo: Položaj linij, kjer je primerjano hitrostno polje; hI = –0,8 m, hII = –0,9 m, hIII = –1,8 m. Desno: Položaj linij, kjer je primerjano temperaturno polje; vI = 0,0 m (sredina), vII = 0,07 m (površina).

not known; however, several reasons why the results are not identical might be identified: the solution procedure, e.g., the energy equation in the commercial code is solved iteratively and the temperature is obtained directly from the equation, whereas in our method, the enthalpy equation is solved first and the temperature is obtained by solving the enthalpy-temperature relationship. Another reason might lie in the differences between the methods, e.g., in the commercial code a second-order upwind technique is used, whereas in our case an adap-
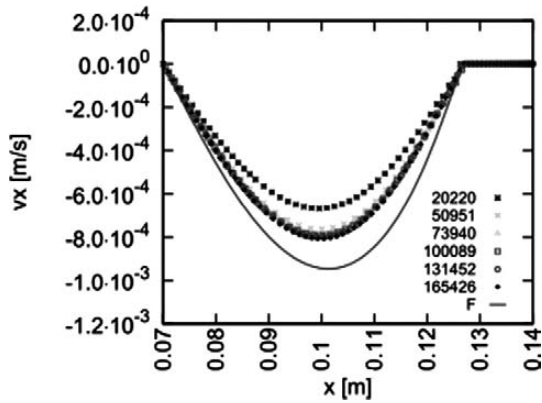
Figure 5: Horizontal-velocity profiles at vertical position hI = –0.8 m, at the top boundary of the magnetic field
Slika 5: Profili horizontalne hitrosti na mestu hI = –0,8 m na zgornji meji magnetnega polja
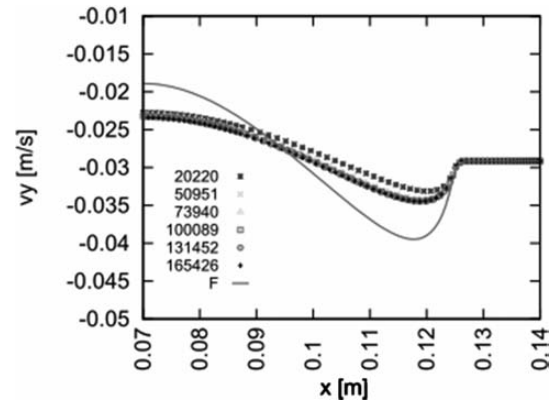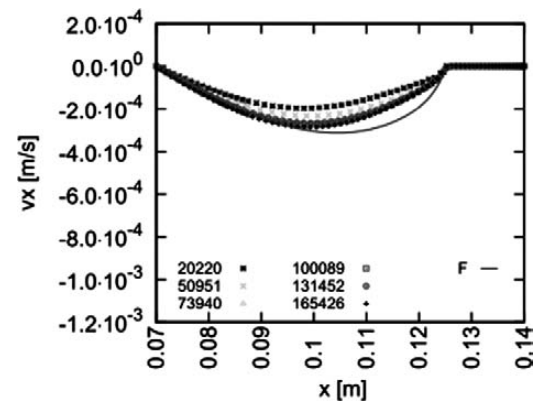

Figure 8: Horizontal-velocity profiles at vertical position hII = –0.9 m, at the bottom boundary of the magnetic field
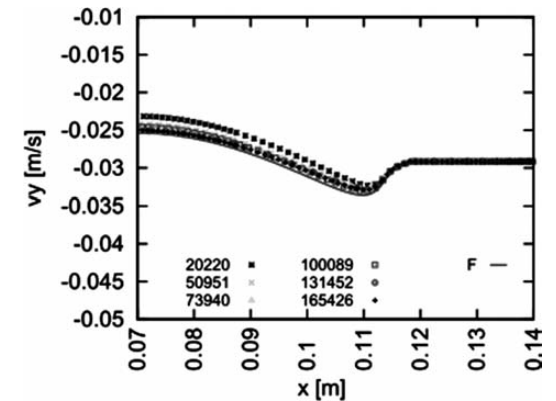**Slika 8:** Profili horizontalne hitrosti na mestu hII = –0,9 m na spodnji meji magnetnega polja
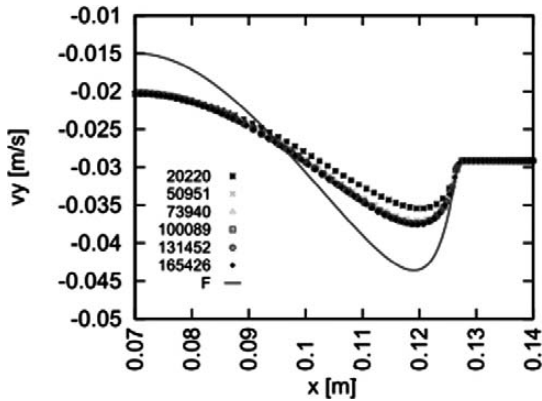
Figure 6: Horizontal-velocity profiles at vertical position hI = –0.8 m, at the top boundary of the magnetic field
Slika 6: Profili horizontalne hitrosti na mestu hI = –0,8 m na zgornji meji magnetnega polja
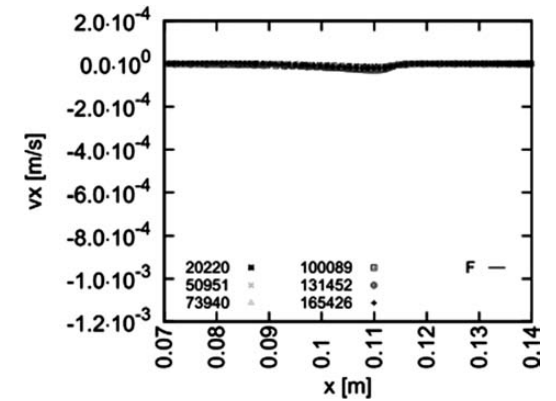
Figure 9: Horizontal-velocity profiles at vertical position hIII = –1.8 m, at the end of the computational domain
Slika 9: Profili horizontalne hitrosti na mestu hIII = –1,8 m na koncu računske domene

Figure 7: Horizontal-velocity profiles at vertical position hII = –0.9 m, at the bottom boundary of the magnetic field
Slika 7: Profil horizontalne hitrosti na mestu hII = –0,9 m na spodnji meji magnetnega polja

Figure 10: Horizontal-velocity profiles at vertical position hIII = –1.8 m, at the end of the computational domain
Slika 10: Profili horizontalne hitrosti na mestu hIII = –1,8 m na koncu računske domene
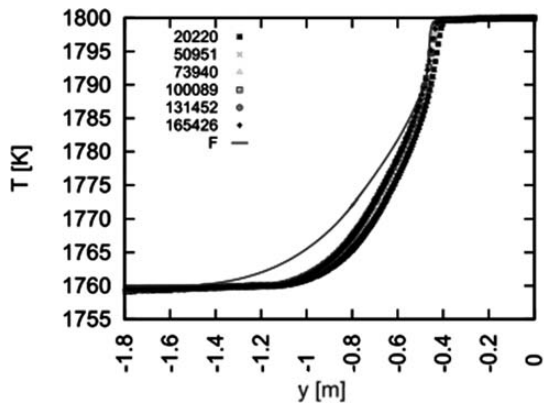
Figure 11: Temperature layout at position vI = 0.0 m, at the centre of the mold
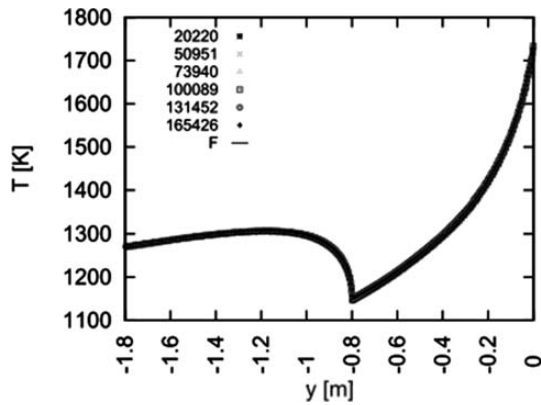**Slika 11:** Potek temperature na mestu vI = 0,0 m v središču kokile

Figure 12: Temperature layout at position vII = 0.07 m, at the mold wall
Slika 12: Potek temperaturnega polja na mestu vII = 0,07 m na steni kokile

tive upwind technique is used. Despite the differences in the formulation, identical results are obtained in very simple test cases; however, slight differences appear when the examples become very complicated, like in the case of continuous casting of steel, where the turbulent-

flow, heat-transfer and magnetic-field equations are strongly coupled.

The agreement between the temperature fields calculated with the commercial code and those calculated with the LRBFCM is better for the outer wall, where the shell has already solidified, than for the centre of the billet, where the liquid metal has not yet solidified.
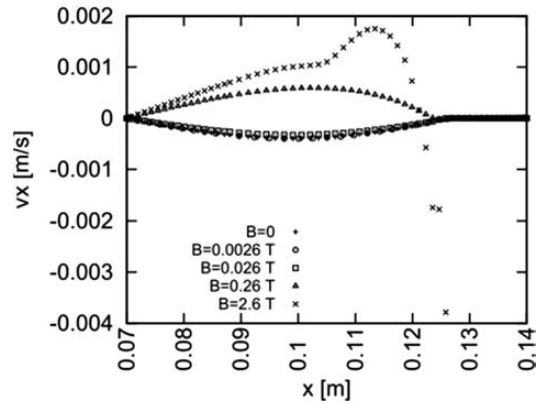

Figure 14: Velocity layout at position vI = –0.8 m
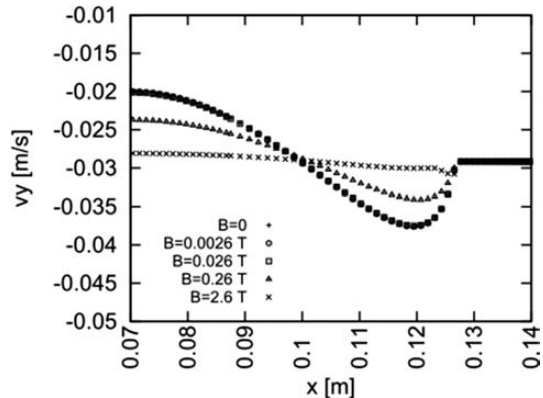**Slika 14:** Potek hitrostnega polja na mestu vI = –0,8 m

Figure 15: Temperature layout at position hII = –0.9 m, at the centre of the mold
Slika 15: Potek temperature na mestu hII = –0,9 m, v središču kokile

Figure 13: Velocity layout at position vI = –0.8 m, at the top edge of the applied magnetic field
Slika 13: Potek hitrostnega polja na mestu vI = –0,8 m na zgornjem robu apliciranega magnetnega polja
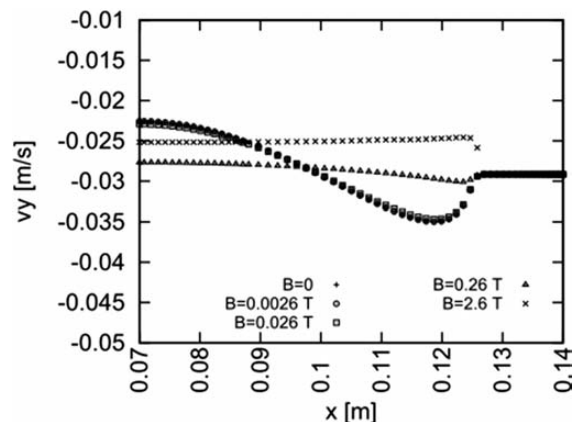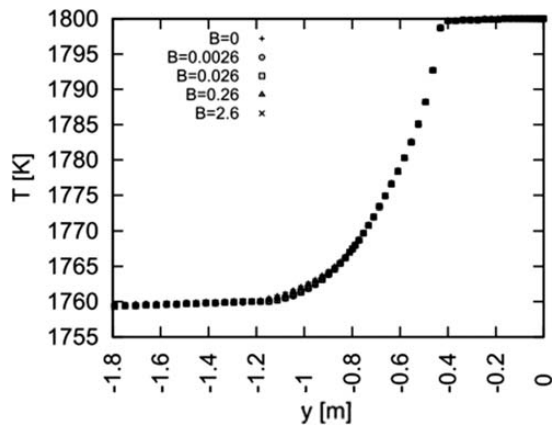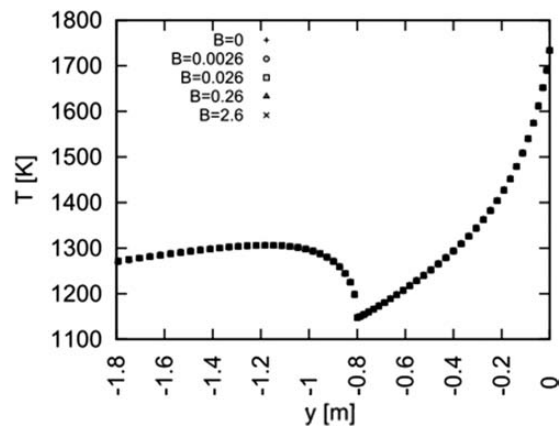

Figure 16: Velocity layout at position hIII = –1.8 m, at the centre of the mold
Slika 16: Potek hitrosti na mestu hIII = –1,8 m na spodnjem robu apliciranega magnetnega polja

Figure 17: Temperature layout at position vI = 0.0 m, at the centre of the mold
Slika 17: Potek temperaturnega polja na mestu vI = 0,0 m v središču kokile

Figure 18: Temperature layout at position vII = 0.07 m, at the mold wall
Slika 18: Potek temperaturnega polja na mestu vII = 0,07 m na steni kokile

Finally, the velocity and temperature profiles were compared for different magnetic-field strengths at different vertical (velocity) and horizontal (temperature) positions. As can be seen in **Figures 13** to **16**, velocity profiles do not change much, when a weak magnetic field (0.0026 T or 0.026 T) is applied, being only slightly different from the velocity profiles obtained with no magnetic field. An application of a weak magnetic field in the x direction causes the velocity in the x direction to increase (**Figures 13** and **14**) and the velocity in the y direction to decrease (**Figures 15** and **16**). However, an application of a strong magnetic field (0.26 T or 2.6 T) alters the velocity profiles and can even change the direction of the flow.

The effect of the externally applied magnetic field on the temperature field is less pronounced. As can be seen in **Figures 17** and **18**, the temperature is slightly raised in the area of the application of the magnetic field.

6 CONCLUSIONS

In this paper, the initial numerical calculations of continuously cast steel under the influence of a magnetic field are presented and compared to the commercial FVM-based computational fluid-dynamics (CFD) code Fluent.[23] The LRBFCM method gives similar results as the commercial code; it is fully flexible, requiring no mesh generation, and enabling a straightforward inclusion of different turbulence models and constitutive equations. In the future, a more realistic magnetic field will be incorporated into the model and a realistic curved geometry of the caster will be assumed. Several sensitivity studies, in terms of the magnitude of an externally applied magnetic field and the position of the coils producing the magnetic field, will be performed. Finally, the species-conservation equation will be added in order to account for the macro-segregation.

7 REFERENCES

[1] W. R. Irwing, Continuous Casting of Steel, The Institute of Materials, London 1993
[2] Steel Statistical Yearbook 2013, World Steel Association, Brussels 2013
[3] B. Šarler, R. Vertnik, A. Z. Lorbiecka, I. Vušanović, B. Senčič, Anwendung eines Stranggieß-Simulationsmodells bei Štore Steel–II, BHM Berg- und Hüttenmännische Monatshefte, (**2013**), 1–9, doi: 10.1007/s00501-013-0147-7
[4] B. Zhao, B. G. Thomas, S. P. Vanka, R. J. O'Malley, Metall. Mater. Trans. B, 36 (**2005**) 6, 801–823
[5] M. R. Aboutalebi, M. Hasan, R. I. L. Guthrie, Metall. Mater. Trans. B, 26 (**1995**) 4, 731–744
[6] D. S. Kim, W. S. Kim, K. H. Cho, ISIJ Int., 40 (**2000**) 7, 670–676
[7] K. G. Kang, H. S. Ryou, N. K. Hur, Numer. Heat Trans. A, 48 (**2005**) 5, 461–481
[8] N. Kubo, T. Ishii, J. Kubota, T. Ikagawa, ISIJ Int., 44 (**2004**) 3, 556–564
[9] C. H. Moon, S. M. Hwang, Int. J. Numer. Meth. Eng., 57 (**2003**) 3, 315–339
[10] B. Šarler, R. Vertnik, Comput. Math. App., 51 (**2006**) 8, 1269–1282
[11] D. C. Wilcox, Turbulence Modeling for CFD, DCW Industries, Inc., California 1993
[12] W. D. Bennon, F. P. Incropera, Numer. Heat Transf. A-Appl., 13 (**1988**) 3, 277–96

[13] K. Abe, T. Kondoh, Y. Nagano, Int. J. Heat Mass Transf., 37 (**1994**) 1, 139–51

[14] B. Šarler, R. Vertnik, K. Mramor, IOP Conference Series: Mater. Sci. Eng., 33 (**2012**) 1, 12012–12021

[15] A. Chorin, Math. Comput., 22 (**1968**) 104, 745–762

[16] H. Lin, S. N. Atluri, CMES (Comput. Model. Eng. Sci.), 1 (**2000**) 2, 45–60

[17] R. Vertnik, B. Šarler, Int. J. Cast Metal. Res., 22 (**2009**) 1–4, 311–313

[18] R. Vertnik, B. Šarler, EABE [online] 2014 [cited 2014-01-02]. Available from World Wide Web: http://dx.doi.org/10.1016/j.enganabound.2014.01.017

[19] M. D. Buchmann, Radial Basis Function: Theory and Implementations, Cambridge University Press, Cambridge 2003

[20] R. Franke, Math. Comput., 38 (**1982**) 157, 181–200

[21] K. Mramor, R. Vertnik, B. Šarler, CMES (Comput. Model. Eng. Sci.), 92 (**2013**) 4, 327–352

[22] K. Mramor, R. Vertnik, B. Šarler, CMC (Comput. Mater. & Continua), 36 (**2013**) 1, 1–21

[23] ANSYS® Fluent, 6.1, ANSYS, Inc.